AIAA JOURNAL
Vol. 36, No. 11, November 1998

Uncertainty Estimates for Temperature-Sensitive Paint Measurements with Charge-Coupled Device Cameras

L. N. Cattafesta III* and T. Liu*
High Technology Corporation, Hampton, Virginia 23666
and
J. P. Sullivan†
Purdue University, West Lafayette, Indiana 47906

Temperature-sensitive paints (TSPs) have become a popular technique for the measurement of surface temperature. Consequently, uncertainty estimates are essential. Whereas TSP is similar in many respects to pressure-sensitive paint (PSP), there are some important distinctions. In particular, TSP is not sensitive to pressure, although PSP is sensitive to temperature. Therefore, a significant error source in PSP intensity measurements is absent in TSP applications. An uncertainty analysis is presented of luminescent TSP intensity measurements with charge-coupled device cameras. Elemental bias and precision error sources are described in detail, and techniques to estimate their magnitude are given for both standard-video and scientific-grade camera systems. Example applications of the technique and uncertainty analysis to swept-wing and swept-cylinder models in supersonic flow are presented. It is shown that error estimates are quite dependent on the system and test configurations. However, the relative motion between model and illumination source(s) is often the dominant error term. A technique to minimize this effect is described.

Nomenclature

B = bias error
I = luminescence intensity
I_a = absorption intensity
k = paint calibration constant, °C
M = Mach number
P = precision error
Re = Reynolds number
T = temperature
U = uncertainty
α = angle of attack
ΔT = temperature change, °C
θ = error sensitivity coefficient
ρ = correlation coefficient
τ = time, s
Φ = efficiency of paint layer

Subscripts

b = bias
D = diameter
p = precision
r = reference conditions
0 = absolute zero temperature
∞ = freestream conditions

Introduction

TEMPERATURE-SENSITIVE paints (TSPs), which are similar in many respects to pressure-sensitive paints (PSPs), have been developed by several research groups to measure wind-tunnel model surface-temperature distributions.[1–4] The application of PSP and TSP to aerodynamic applications has been reviewed in detail by Liu et al.[5] The method can provide detailed temperature measurements at relatively low cost. It should be noted that TSP has many similarities to thermographic phosphors, which have been recently reviewed by Allison and Gillies.[6]

Pressure and temperature paints are based on the mechanism of photoluminescence, in which a probe molecule, promoted to an excited electronic state by absorbing a photon of appropriate energy, returns to its ground state by emitting a lower-energy photon. In addition, the data-reduction processes are similar. However, there are some important distinctions. First, whereas the effects of pressure on luminescence intensity are often described using the Stern–Volmer relation,[7] the molecular physics are different for TSP, and they are described in detail by Rabek.[8] Instead of the luminescence being quenched by oxygen as in PSP, radiationless deactivation reduces the luminescence intensity in TSP via thermal quenching as the temperature increases. In particular, the increased frequency of collisions with higher temperature improves the probability of deactivating the probe molecule (as opposed to the molecule emitting a photon). Thus, the magnitude of the luminescence intensity is inversely proportional to temperature in TSP.

Second, PSP is sensitive to both pressure and temperature, whereas TSP is sensitive only to temperature. Indeed, much of the uncertainty of PSP measurements can be due to temperature effects, with the uncertainty due to other error sources being negligible by comparison.[9] Because this is not the case for TSP, the accuracy of TSP measurements must be assessed separately. The purpose of this paper is to provide a framework for estimating the uncertainty of TSP luminescence intensity measurements with charge-coupled device (CCD) cameras. The particular TSP used in this study is a proprietary McDonnell Douglas ruthenium compound mixed in enamel Krylon® paint; however, the analysis is applicable to the many TSPs that have been documented in the literature.[1]

The paper is organized as follows: The experimental method is described, followed by a general uncertainty analysis, in which the overall uncertainty is considered and not the details of the bias and precision error components. The elemental bias and precision error components of both standard-video and scientific-grade CCD cameras are discussed in detail in the next section, and techniques for estimating their magnitudes are given. Next, sample applications of TSP to supersonic swept-cylinder and swept-wing models, as well as corresponding uncertainty estimates, are provided. These results provide insight into an often dominant error source and suggest an alternate method to minimize its influence. This is followed by some conclusions.

Presented as Paper 95-2193 at the AIAA 26th Fluid Dynamics Conference, San Diego, CA, June 19–22, 1995; received Dec. 8, 1997; revision received July 15, 1998; accepted for publication July 29, 1998.

*Research Scientist, Experimental & Instrumentation Group, 28 Research Drive. Member AIAA.
†Professor of Aerodynamics, School of Aeronautics and Astronautics. Member AIAA.

Experimental Method

This section describes the data acquisition and reduction methods for image-based luminescent paint with CCD cameras. Note that other data acquisition and reduction methods are available. For example, Campbell et al.[1] explain how the measurement of either the paint fluorescence lifetime or the phase shift between intensity-modulated excitation and luminescence signals can be used to determine temperature. Nonetheless, an image-based measurement system remains the most popular method because it can easily provide a global surface temperature distribution, whereas the other methods are currently constrained to point measurements because of instrumentation limitations.

Before a test, the model is painted with temperature paint and is sanded to remove any roughness. Registration marks are then placed on the painted model surface, the exact locations of which must be precisely measured. (The purpose of these marks will be explained subsequently.) Currently, we use rub-on dots that do not fluoresce. To eliminate any roughness effects that may have been introduced by the registration marks, a gloss clear coat is sometimes applied. Finally, the model is polished to the desired surface finish.

During a test, data are acquired as follows: The model is illuminated by filtered light from an appropriate stable source. Luminescence occurs at a higher wavelength, the intensity of which is measured by a CCD camera fitted with a bandpass filter that transmits only the red-shifted light emitted by the paint. Care is taken to eliminate all other stray light.

The magnitude of the luminescence is related to the paint temperature, luminophore concentration, and source irradiance. Unfortunately, the portion of the luminescence signal that is due to temperature is often of the same order as these other effects. Hence, an image-ratio method is employed to isolate the influence of temperature. In this method, the paint temperature under test conditions is related to the ratio of two images of the model obtained under different conditions: one at a known reference temperature condition (usually corresponding to a no-flow or wind-off condition) and another at run conditions. A ratio of these two images, each one corrected for a zero offset by subtracting a dark image of the unexposed CCD, thus eliminates the portion of the luminescence signal that is common to the two images. In the ideal case, all that remains is a temperature image, the values of which are obtained from a calibration curve.

In wind-tunnel applications, however, the ideal case is rarely achieved. For example, the model usually deflects and/or deforms under load. At a minimum, the reference and run images must be realigned or registered before the images are divided. Thus, the purpose of the registration marks is to provide a mechanism for the images to be realigned. An additional complication of model motion/deformation that can occur is that the illumination pattern on the model surface may change between the reference and run images. This effect is not corrected for in the image registration process. Thus, in general, the illumination pattern on the model surface should be measured in situ, although this is rarely done in practice. The magnitudes of these and other errors, therefore, have a first-order effect on the accuracy of the measurement and are discussed in detail in subsequent sections.

General Uncertainty Analysis

Performing an uncertainty analysis of a complex measurement system can be a daunting task. The approach suggested by Coleman and Steele[10] is to first perform a general uncertainty analysis in which the details of the bias and precision error components are ignored. This approach often provides insight into the accuracy requirements imposed on the measurement system.

For TSP, the intensity of the luminescence emitted by the paint, I, is proportional to the intensity of the light absorbed by the paint, I_a. The constant of proportionality is called the quantum yield or efficiency, $\Phi \equiv I/I_a$. Liu et al.[5] show that the general Arrhenius relation governing a TSP is given by

$$\ln\left[\frac{I\cdot(I_0-I_r)}{I_r\cdot(I_0-I)}\right]=\frac{E}{R}\cdot\left(\frac{1}{T}-\frac{1}{T_r}\right) \tag{1}$$

where E is the Arrhenius activation energy; R is the universal gas constant; and I, I_r, and I_0 are the respective luminescence intensities at temperatures T, T_r, and 0. Under normal circumstances, T is close to T_r, such that the factor $(I_0-I_r)/(I_0-I)$ is nearly unity. Thus, Eq. (1) may be expressed in an equivalent exponential form:

$$I = I_r\cdot\exp\left[\frac{-(T-T_r)}{k}\right] \tag{2}$$

in which the constant k ($=R\cdot T\cdot T_r/E$) amounts to a characteristic paint constant at a nominal operating temperature T. [An even more general expression replaces intensity in Eq. (2) with quantum yield.] Equation (2) is a convenient form because it possesses the property $I\cdot e^{T/k}=I_r\cdot e^{T_r/k}=\text{const}$; thus, a pretest calibration is valid provided that an appropriate reference set (I_r, T_r) is used. Finally, note that, although not universal, Eq. (2) does accurately represent a wide class of TSPs over a certain temperature range. The interested reader is referred to the paper by Campbell et al.[1] for intensity-calibration curves of several TSPs.

The first step in a general uncertainty analysis is to solve for the desired quantity in terms of the other quantities. Very often, we are interested only in the change in temperature from the reference condition

$$\Delta T_r = T - T_r = k\cdot\ln\frac{\Phi_r}{\Phi} = k\cdot\ln\frac{I_r\cdot I_a}{I\cdot I_{a,r}} \tag{3}$$

where we have used the definition of Φ to obtain a data-reduction equation in terms of either known or measurable quantities.

Equation (3) is written in a general form in which the absorption intensity is included. Although it is often assumed that the source irradiance is constant, such that $I_a/I_{a,r}=1$, the assumption is only an approximation and contributes to the uncertainty. To accurately determine its justification, the source irradiance must be at least monitored. Alternatively, this could be accomplished in situ by using a two-color paint, one that contains both temperature and reference luminophores.[11]

Following the standard root-sum-square procedure outlined by Coleman and Steele,[10] the absolute uncertainty associated with ΔT_r is given by

$$U_{\Delta T_r}^2=\left(\frac{\partial\Delta T_r}{\partial I}U_I\right)^2+\left(\frac{\partial\Delta T_r}{\partial I_r}U_{I_r}\right)^2+\left(\frac{\partial\Delta T_r}{\partial I_a}U_{I_a}\right)^2+\left(\frac{\partial\Delta T_r}{\partial I_{a,r}}U_{I_{a,r}}\right)^2+\left(\frac{\partial\Delta T_r}{\partial k}U_k\right)^2 \tag{4}$$

where U denotes uncertainty. Substituting in the partial derivatives and simplifying gives

$$U_{\Delta T_r}^2=k^2\left[\left(\frac{U_I}{I}\right)^2+\left(\frac{U_{I_r}}{I_r}\right)^2+\left(\frac{U_{I_a}}{I_a}\right)^2+\left(\frac{U_{I_{a,r}}}{I_{a,r}}\right)^2\right]+\Delta T_r^2\left(\frac{U_k}{k}\right)^2 \tag{5}$$

The coefficient of each relative uncertainty term, U_X/X, indicates the relative importance of each term. Thus, the sensitivity to each intensity term is k, whereas that due to the calibration error term is ΔT_r. Provided that $k>\Delta T_r$, the measurement is more sensitive to errors in intensity measurements and source drift than to calibration errors. Note that k is related to the normalized paint sensitivity $[(\Delta T_r/I)\cdot(\partial I/\partial\Delta T_r)=-(\Delta T_r/k)]$. In particular, by inspection of Eq. (2), k can be viewed as the $1/e$ temperature change, i.e., the temperature change corresponding to a $1/e$ change in luminescence intensity. Once a paint is selected based on a nominal operating temperature range, it is clear that smaller values of k increase the paint sensitivity and decrease the uncertainty.

These ideas are shown in Figs. 1 and 2, which show a typical TSP calibration curve near ambient temperature and absolute uncertainty estimates, respectively. Figure 1 shows the influence of the paint constant k on the calibration curve. A lower value of k increases the slope of the calibration curve, improving the sensitivity of the instrument. Figure 2 uses the fitted calibration constant $k=37.7^\circ$C

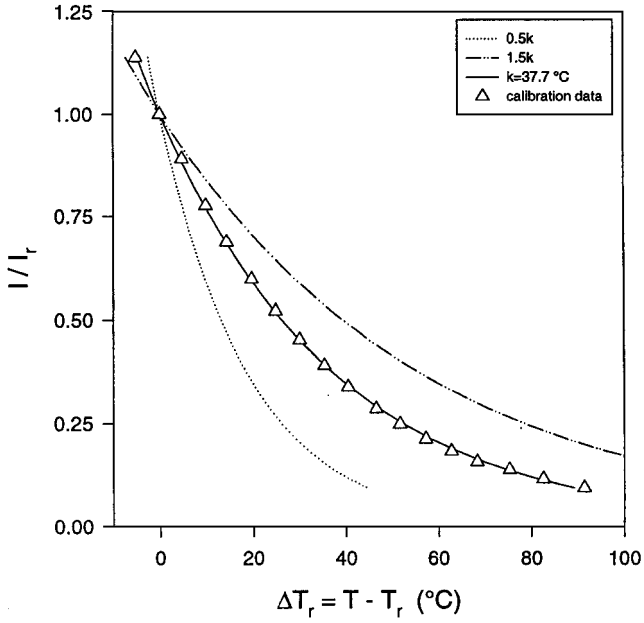

Fig. 1 TSP calibration curves.

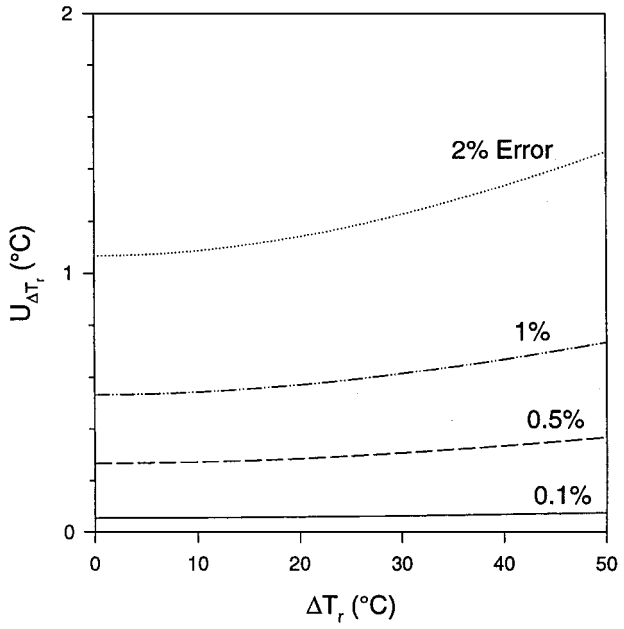

Fig. 2 Absolute uncertainty estimates for TSP.

and shows the calculated uncertainty using Eq. (5) vs temperature change as a function of relative error in I, I_r, and k (under the ideal condition of zero error in I_a and $I_{a,r}$). These results show that, to keep absolute errors below 0.5°C, an accuracy of better than 1% in each measured quantity is required.

Detailed Uncertainty Analysis

The next step is to conduct a detailed uncertainty analysis in which we consider separately the propagation of bias and precision errors into the result. A bias error is a fixed or systematic error, whereas a precision or random error can be reduced by multiple readings. Bias and precision errors are distinguished due to their differing behavior. Following the approach of Coleman and Steele,[10] a 95% confidence-interval estimate is required for each bias and precision error component of each variable that appears in the data reduction equation. The approach taken here is to first identify and estimate the elemental bias and precision error components. These elemental errors are then combined to produce 95% confidence-interval bias and precision estimates in accordance with Eq. (5). These error sources are described in detail next.

Elemental Bias and Precision Error Sources

For the present discussion, the measured variables are taken as k, I, I_r, I_a, and $I_{a,r}$, despite k itself being a derived quantity. Table 1 lists elemental error sources that contribute either to the determination of k, i.e., from the calibration, or to any of the intensity measurements. It also includes suggested methods to quantify them. The list is not exhaustive but rather includes, from our experience, significant error sources.

Aspects associated with the temperature calibration are considered first. The accuracy of the secondary temperature standard may be used to estimate its bias but is usually negligible compared with other sources of error when one is concerned with measuring temperature changes. Two other bias sources require careful attention: photodegradation and temperature hysteresis.[12] Photodegradation of the fluorescent paint occurs when the paint is exposed to the illumination light. The photodegradation process depends on illumination intensity, exposure time, and the paint itself. To minimize errors in applications, the exposure time in a single test should be as short as possible. Calibrations before and after a test sequence can quantify the exact extent of the photodegradation. Fortunately, Liu et al.[12] have shown that normalized calibration curves approximately collapse to a single curve, minimizing its influence on the calibration. However, the signal-to-noise ratio (SNR) for a severely photodegraded paint decreases because the signal becomes weaker.

Hysteresis is a feature characterized by a change in the calibration curve when the paint is first heated above its glass temperature.[13] The temperature hysteresis is related to the polymer structural transformation from a hard and relatively brittle state to a soft and rubbery one when its temperature exceeds the glass temperature. Because the thermal quenching of fluorescence in a brittle condition is different from that in a rubbery state, the temperature dependence changes after it is heated beyond the glass temperature. In practice, the paint should be preheated once to a temperature above the glass temperature, prior to calibration, before it is used as a sensor for quantitative measurements.

The contributions of elemental bias and precision errors to intensity measurements are considered next. Either two (I and I_r) or four (I, I_r, I_a, and $I_{a,r}$) such measurements are made. For the case in which only the paint luminescence intensity is measured in reference and run images, temporal variations in the source introduce errors. These include random, short-term fluctuations (with a timescale of order equal to the exposure time) and long-term, systematic drift between acquisition of the reference and run images. In an effort to quantify these, a benchtop experiment showed that a typical constant-current halogen source exhibits drift of about 0.1% over the duration of a 30-min test and short-term fluctuations of about 0.2%. An optical-feedback halogen source, in which the irradiance is monitored and controlled in a feedback loop, exhibits approximately the same drift but reduces the short-term fluctuations to immeasurable levels.

In the case of four intensity measurements, the source irradiance and its distribution over the model surface are also measured (as described earlier). The result is that the effect due to source drift is eliminated. This technique has an added benefit. Because relative motion between the model and source can occur due to model deflections, the irradiance incident on the model surface can change slightly between the reference and run images. Information about the distribution of this illumination pattern can be used to correct for this change. Of course, this process itself has errors associated with its implementation (which may or may not be negligible). In addition, this technique suffers from the drawback that four intensity measurements are required instead of two. For the results presented later, only I and I_r have been measured. Thus, the accuracy of this approach has yet to be evaluated.

As indicated in Table 1, CCD cameras are subject to three types of noise: photon shot noise, dark current, and preamplifier or readout noise. It is primarily in this area where a scientific-grade, e.g., a high-resolution, cooled, digital camera excels compared with a conventional video camera, as explained next.

Photon shot noise is an unavoidable quantum effect in which the number of photons collected by a CCD from a steady source over a time interval is governed by a Poisson distribution. Here the rms

Table 1 Elemental bias and precision error sources

Error source	Bias (B) or precision (P)	Estimate error from
Calibration curve fit	P	2σ of least-squares fit
Standard used in calibration	B	Manufacturer specifications
Photodegradation of paint	B	Calibrate before and after a test
Temperature hysteresis	B	Deviation between repeated calibrations
Random source fluctuations	P	Measure in benchtop apparatus or in situ
Systematic source drift	B	Measure in benchtop apparatus or in situ
Photon shot noise	P	2/(signal strength in e.u.)$^{1/2}$
Dark current	P	Camera specifications
Preamplifier noise	P	Camera specifications
Digitizer bias	B	Subtract dark image from I and I_r
Digitizer resolution	B	$\pm\frac{1}{2}$ least significant bit/I
A/D nonlinearities	B	CCD specifications or intensity calibration
Pixel-gain variation	B	Zero without image registration; with image registration, need flat-field measurements
Image registration errors Location of registration marks in pixel coordinates, location of registration marks in model coordinates, least-squares-fit error Interpolation error	B	Difficult to isolate: can perform uncertainty analysis of image registration method
Random model vibration	P	Configuration dependent, measure in situ
Relative motion between source and model	B	$\sqrt{\left(\frac{\partial I_r}{\partial x}\frac{\Delta x}{I_r}\right)^2+\left(\frac{\partial I_r}{\partial y}\frac{\Delta y}{I_r}\right)^2}$
Ambient light	B	Exposure with light source off and shutter open
Source and camera filters overlap	B	Filters' spectral transmission specifications

Table 2 Scientific-grade CCD camera vs standard-video CCD camera

Parameter	Front-illuminated scientific-grade CCD	Standard video
Gray-scale resolution, bit	14	8
Linearity	$\pm 2/I$	$\pm 2/I$
Pixels	512×512	512×480
Readout noise *NP*, e.u. rms	35	200
Dark current *ND*, e.u./s	0.7	20,000
Quantum efficiency at 500 nm η, %	10–25	10
Exposure τ, s	~10	1/60
Full-well capacity, e.u.	~345,000	~40,000

noise is equal to the square root of the signal. (The units of the noise are electron units.)

Thus, the SNR is $\sqrt{I}$, and the highest SNR is obtained when the full-well capacity of the CCD is utilized. To accomplish this in scientific-grade cameras, the shutter is opened long enough (usually on the order of seconds) to saturate the analog-to-digital (A/D) converter at the minimum temperature to be measured. For long exposures in low-light-level situations, dark current, a thermally induced current, becomes important. Fortunately, it can be significantly reduced by cooling the CCD head, as is done in scientific-grade cameras. Preamplifier noise is generated by the amplifier on the CCD chip and sets the detection limits of a cooled CCD at low-light conditions. Table 2 shows typical values of these parameters for both the 14-bit, i.e., $I_{\max} = 2^{14}$, scientific-grade and 8-bit, i.e., $I_{\max} = 2^8$, standard-video camera used in this study. The noise levels are substantially higher for conventional video cameras.

In addition to these random errors, the intensity measurements are subject to a number of bias errors. The repeatable drift of the light source has already been discussed. The digitizer bias or zero-offset error is typically corrected for by subtracting a dark image, an image acquired with the camera shutter closed, from both the reference and run images. The A/D nonlinearities also contribute to the error. Here, the scientific-grade CCD is extremely linear, compared with the typical 1% variation in standard-video cameras.

As mentioned earlier, the optical setup requires separate filters for the light source and the camera. For the temperature paint used in this study, the transmission range of these filters is quite close, unlike PSP applications, almost overlapping at 500 nm. It is important that these filters do not overlap. Similarly, stray light should be eliminated. Note that the stray light is present in both the reference and the run images, and the error is, therefore, correlated. A detailed discussion of correlation errors is provided in the next section.

As shown by Morris et al.,[14] even scientific-grade CCDs have measurable pixel-to-pixel gain variations. When the CCD is illuminated with a uniform field of light (using an integrating sphere whose output is filtered with the same bandpass filter used for luminescence detection), variations of $\pm 1\%$ are typical. CCD camera literature suggests that this value is even higher for video cameras, although the exact magnitude varies with CCD type.

Nonetheless, this variation introduces a bias error when the same pixels are not divided in the reference and run images. Assuming a linear A/D, this effect cancels when the same pixels are divided. However, when image registration is used to realign the reference and run images, the error introduced by this effect can be significant. Morris et al.[14] describe a standardized procedure that uses a flat-field calibration of the camera (again using an integrating sphere, filter, and camera lens) to correct for the pixel gain variation. We have used this technique to obtain an order-of-magnitude reduction to $\pm 0.1\%$. Note that, when image registration is used in an attempt to minimize errors due to image misalignment but a flat-field correction is not used, the overall error may actually increase as a result of pixel gain variations.

Image registration techniques are discussed in detail by Bell and McLachlan[15] and also by Donovan et al.[16] A popular method is a least-squares polynomial warping technique in which the locations of the registration marks are matched in both the reference and the run images. Here, rms errors on the order of a small fraction of a pixel are routinely achieved. Unfortunately, it is difficult to isolate the contribution of the image registration error to the overall measurement uncertainty. Table 1 lists the dominant error sources associated with image registration. One may perform a separate uncertainty analysis of this process, although this has not been attempted here. It is our experience that, if the relative motion between the reference and the run images is less than one pixel and a reliable flat-field calibration is unavailable, then image registration is not recommended.

Perhaps the single largest contribution to the bias error (and the overall error for scientific-grade cameras) is that due to relative motion between the model and the source. Again, the relative motion has a random component, the magnitude of which is configuration dependent, and a steady or systematic component. Model motion effectively alters the luminescence intensity by changing the

illumination pattern on the model surface. The effect is most pronounced in regions of large luminescence intensity variations in the reference image, e.g., near the limits of a field of view.

The preceding observation is used to estimate the magnitude of the error due to relative model motion, as shown in Table 1. In particular, this error is estimated using the normalized intensity gradient in the reference image coordinate system (x, y):

$$B_{\text{motion}} = \sqrt{\left(\frac{\partial I_r}{\partial x}\frac{\Delta x}{I_r}\right)^2 + \left(\frac{\partial I_r}{\partial y}\frac{\Delta y}{I_r}\right)^2} \tag{6}$$

where Δx and Δy are 95% estimates of the local model motion in pixels.

Correlated-Error Effects

The overall uncertainty equation derived in the general uncertainty analysis must be modified slightly to account for correlated-error effects. Thus, Eq. (5) becomes

$$U^2 = \sum_{i=1}^{J}\left[\theta_{b_i}^2 B_i^2 + \sum_{k=1}^{J}\theta_{b_i}\theta_{b_k}\rho_{b_{ik}} B_i B_k (1-\delta_{ik})\right] + \sum_{i=1}^{J}\left[\theta_{p_i}^2 P_i^2 + \sum_{k=1}^{J}\theta_{p_i}\theta_{p_k}\rho_{p_{ik}} P_i P_k (1-\delta_{ik})\right] \tag{7}$$

where δ_{ik} is the Kronecker delta function, θ is a sensitivity coefficient, ρ is a correlation coefficient, and B_i and P_i are the 95% bias and precision estimates of the ith variable, respectively.[10]

The two new product terms in Eq. (7) represent correlated errors. Although often zero, these terms are sometimes significant. For example, in a differential measurement, in which two instruments are calibrated with the same secondary standard, the bias of this standard is correlated and will cancel.

In the case of luminescence intensity measurements, the ambient light seen by the camera, as well as the overlap between the source and camera filters, is approximately equal in both the reference and the run images. The correlated bias term in Eq. (7) may be written as $\rho_{b_{ik}} B_i B_k (1-\delta_{ik}) = (1) B_i' B_k'$ for $i \neq k$, where the prime denotes elemental bias error sources that are common to both variables. Then the summation is taken over the number of common elemental bias terms. In the case of the ambient light, for example, one obtains the following expression for the net bias error:

$$k^2\left[(B_I/I)^2 + \left(B_{I_r}/I_r\right)^2\right]_{\text{ambient}} - 2k^2\left[(B_I'/I)\left(B_{I_r}'/I_r\right)\right]_{\text{ambient}} \tag{8}$$

A similar expression is obtained for the filter overlap. However, if it is assumed that

$$B_I/I \cong B_{I_r}/I_r \cong B_I'/I \cong B_{I_r}'/I_r \tag{9}$$

for both ambient light and filter overlap, then the net contributions due to these effects will cancel. The preceding result is only approximate because, in fact, the amount of stray light that is measured by the camera is an absolute amount and not a fixed fraction of the luminescence intensity.

Stated another way, if the measured luminescence intensities are contaminated by the same amount of ambient (or filter-overlapped) light, then instead of determining the ratio I_r/I, one actually obtains $(I_r + \Delta I)/(I + \Delta I)$, where ΔI is the intensity of stray light. If ΔI is negligible compared with both I and I_r, then the error is small. In summary, this means that only a small amount of stray light can be tolerated for high-accuracy measurements.

Quantitative Error Estimates

Now the results of the preceding sections are combined to formulate a rational method for estimating the total uncertainty in the measurement of ΔT_r for each pixel. By way of example, we include the following bias terms: pixel gain variations, CCD nonlinearities, bit resolution, systematic relative motion, and source drift. The contribution of the bias errors to the calibration is assumed to be negligible. The formula for the variance of the 95% bias-error estimate is

$$B_{\Delta T_r}^2 = k^2\left[N\left(B_{\text{gain}}^2 + B_{\text{linear}}^2 + B_{\text{res}}^2\right) + B_{\text{motion}}^2 + B_{\text{drift}}^2\right] \tag{10}$$

where the biases are expressed as relative errors and N is the number of intensity measurements (two or four). For a scientific-grade camera, these quantities are estimated as $B_{\text{gain}} \approx 0$ without image registration, ≈ 0.01 with image registration and without flat field, ≈ 0.001 with image registration and with flat field; $B_{\text{linear}} \approx 2/I$; $B_{\text{res}} \approx 0.5/I$; $B_{\text{drift}} \approx 0$ if I_a and $I_{a,r}$ are measured or are corrected for, else ≈ 0.001; for B_{motion} see Eq. (6).

Similarly, the formula for the variance of the 95% precision-error estimate is

$$P_{\Delta T_r}^2 = \frac{1}{N_{\text{images}}}\left[k^2 \cdot N \cdot \left(P_{\text{vib}}^2 + P_{\text{source}}^2 + P_{\text{dark}}^2 + P_{\text{shot}}^2 + P_{\text{preamp}}^2\right) + \Delta T_r \cdot P_k^2\right] \tag{11}$$

where again relative precision errors are used and N_{images} is the number of images averaged to reduce the random error. As before, N is the number of intensity measurements. Note that the precision error due to model vibration, P_{vib}, is dependent on the configuration, whereas that due to source fluctuations, P_{source}, is about 0.2% for a constant-current source or is entirely negligible if feedback is employed. Following guidelines in Ref. 17, the noise terms are estimated as

$$P_{\text{dark}} = 2 \cdot ND\frac{\text{e.u.}}{\text{s}}\frac{2^{n\,\text{bits}}\text{ADU}}{\text{FWC e.u.}}\frac{\tau\ \text{s}}{I\ \text{ADU}} \tag{12a}$$

$$P_{\text{shot}} = \frac{2\sqrt{I}\,\text{e.u.}}{I\ \text{e.u.}} = \frac{2}{\sqrt{I}} \tag{12b}$$

$$P_{\text{preamp}} = 2 \cdot NP\,\text{e.u.} \cdot \frac{2^{n\,\text{bits}}\text{ADU}}{\text{FWC e.u.}}\frac{1}{I\ \text{ADU}} \tag{12c}$$

where ND is the dark current, $n$bits is the number of bits in the A/D, τ is the exposure time, FWC is the full-well capacity of the CCD in electron units, I represents the measured intensity expressed in A/D units (ADU), and NP is the preamp noise in reciprocal electron units. Note that the preceding relations provide 2σ estimates normalized by the signal I.

Table 2 provides typical values for these parameters for both a scientific-grade and a standard-video camera. Using these values and a midrange intensity ($I = 8192$ and 128 for the scientific-grade and standard-video camera, respectively), we obtain the following comparison: $P_{\text{dark}} = 8.1 \times 10^{-5}$ vs 0.033, $P_{\text{shot}} = 0.022$ vs 0.177, and $P_{\text{preamp}} = 4.1 \times 10^{-4}$ vs 0.02. Whereas these values can be reduced by averaging, a standard-video camera is clearly not well suited for accurate measurements.

A 95% confidence-interval estimate for the total uncertainty is obtained from

$$U_{\Delta T_r}^2 = B_{\Delta T_r}^2 + P_{\Delta T_r}^2 \tag{13}$$

where the bias and precision estimates are obtained from Eqs. (10) and (11).

Results and Discussion

This section discusses the application of TSP to transition-detection measurements on two models: a 76-deg swept-cylinder model (diameter = 2.54 cm and length = 35.56 cm) and a 78-deg swept-wing model (length = 38.1 cm) in the NASA Langley Research Center Supersonic (Mach 3.5) Low-Disturbance Tunnel.[18] In particular, sample results are presented, and uncertainty estimates are evaluated at each pixel using Eqs. (10–13). The results presented in the following are for a scientific-grade camera only. As noted earlier, only I and I_r are measured.

Test Cases

To evaluate the effectiveness of the uncertainty analysis, some simple test cases are performed with the swept cylinder. To begin, two single wind-off exposures of the cylinder are acquired in succession. Here, the model is at a uniform temperature and, because there is no flow, the bias error due to relative model motion is zero.

Figures 3a and 3b show the ΔT_r and uncertainty images, respectively. Because the mean temperature equals the reference temperature, Fig. 3a actually represents the true error. Accounting for the

background, the 95% error bounds are $-0.31^{\circ}\text{C} \leq \text{error} \leq 0.29^{\circ}\text{C}$. The uncertainty estimate, computed at each pixel as earlier outlined, varies from 0.23 to 0.57°C, and the average estimate is $\pm 0.30^{\circ}$C. Alternatively, because an uncertainty estimate is obtained for each point in the temperature image, one can calculate the percentage of pixels for which the uncertainty estimates bounds the actual error; this result is 97%. Thus, the uncertainty estimate is consistent with a 95% confidence interval.

A harsher test case is needed to assess the ability of the method to estimate the contribution of the bias errors, most notably that due to systematic relative model motion. To do this, the approximate deflection of the swept-cylinder model is estimated from prior test runs. This deflection is then simulated in a wind-off condition by first acquiring a single reference image, and then after deflecting the model by loading the model mount with weights, a simulated run image is acquired.

Figures 4a and 4b show the ΔT_r and uncertainty images, respectively. The static loading of the model mount is such that the run image effectively moves away from an observer into the page. However, the deflection is less than one pixel in both directions, and so polynomial image registration is ineffective here.

The temperature image, which again is the actual error image, reveals little detail, with the exception of the registration marks, a junction in the model, and the model edges. The uncertainty image emphasizes these regions of potentially large errors and also estimates the magnitude of the errors. Figure 4c shows line plots of ΔT_r and uncertainty estimates extracted from their respective images in Figs. 4a and 4b. These plots show that random errors dominate in the central portion of the image away from model edges but that the model motion causes large bias errors that dominate near the visible edges of the model. The uncertainty analysis clearly defines these regions.

The true error varies from -1.3 to 2.4°C, primarily due to model deflection, whereas the uncertainty estimates vary from 0.23 to about 4°C. The uncertainty estimate bounds the actual error 81% of the time. Although lower than the desired value of 95% coverage, further analysis shows that the uncertainty estimate bounds the error over 95% of the time when the error is less than 1°C. Therefore, it may be concluded that the bias error is underestimated near model edges. Nonetheless, the uncertainty analysis certainly shows the right trends and represents an effective method for evaluating the local quality of a temperature image.

Sample Applications

In flow-on situations, the swept-cylinder model exhibits large temperature variations along its length (due to the large thermal mass of a solid support structure). The TSP results agree with corresponding thermocouple measurements. However, the thermocouples are not calibrated against a secondary standard, and so their estimated uncertainty (approximately $\pm 1^{\circ}$C) is greater than that of the paint measurements.

A sample paint result and corresponding uncertainty image are shown in Figs. 5a and 5b, respectively. The flow conditions are $M_{\infty} = 3.5$ and $Re_D \cong 9.6 \times 10^5$. Three cycles of a standard linear gray-scale look-up table (LUT) are used to increase the contrast in the ΔT_r image. A parabolic-shaped transition region is clearly visible in this image.

Note that in Fig. 5b the regions of large uncertainty are confined to within about 10 pixels of the model edge (ignoring the registration-mark locations). Away from edges, the uncertainty is about $\pm 0.3^{\circ}$C.

An interesting point about this application is that, instead of using a wind-off image as the reference image, a run image at a low Reynolds number, i.e., laminar condition, is used. As a result, the relative motion bias is substantially reduced because the incremental change in model deflection between the two run conditions is small. A similar technique was first suggested by McLachlan et al.[4] for low-speed flows in which run images obtained at two different Mach numbers are used to infer the transition location.

Finally, the results from a swept-wing application are shown in Figs. 6a and 6b. Here the flow conditions are $\alpha = -2$ deg and $Re_{\infty} \cong 13.8 \times 10^6$/m. Again, a three-cycle LUT is used to show

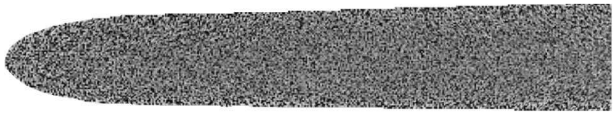

a) ΔT_r image between two successive images

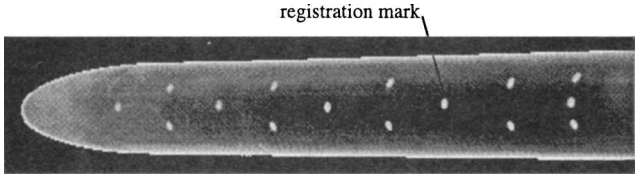

b) Uncertainty image corresponding to ΔT_r image shown in part a

Fig. 3 Results of first test case with swept cylinder that show the variation in temperature between two successive wind-off images.

a) ΔT_r image

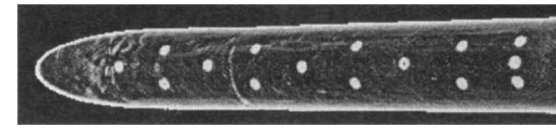

b) Uncertainty image

Fig. 5 TSP results of swept-cylinder test for Mach 3.5 and $Re_D = 9.6 \times 10^5$; three cycles of a standard gray-scale LUT are used for the image in part a.

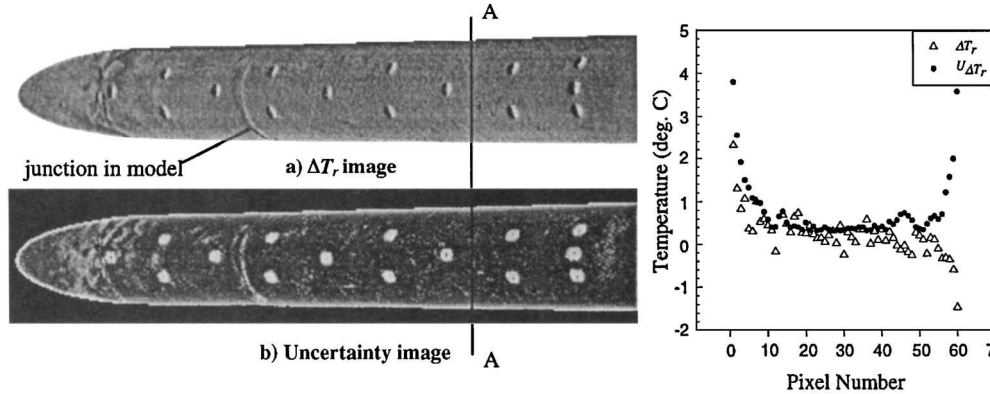

c) Section A–A in parts a and b

Fig. 4 Results of second test case with swept cylinder that show the temperature error introduced by model motion.

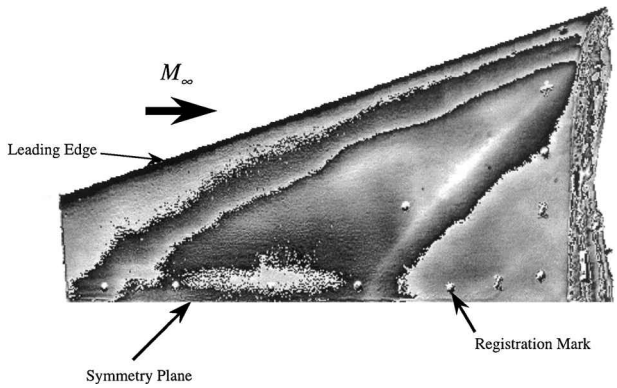

a) ΔT_r image

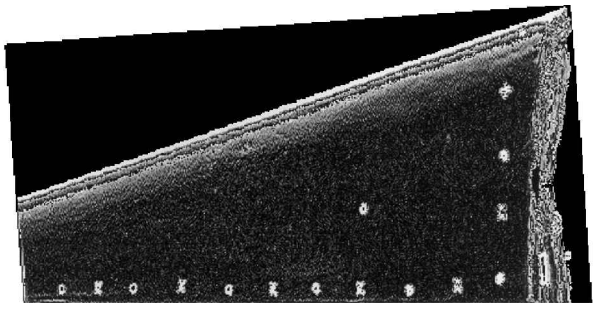

b) Uncertainty image

Fig. 6 TSP results of swept-wing test for angle of attack = − 2, Mach 3.5, and *Re*/m = 13.8 × 10^6; three cycles of a standard gray-scale LUT are used for both images.

the transition front in the ΔT_r image. The transition front is approximately parallel to the leading edge of the model and then turns and becomes almost parallel to the symmetry plane. As with the swept-cylinder application, companion thermocouple measurements agree with the TSP measurements to within the estimated accuracy of the thermocouples ($\pm 1^\circ$C vs about $\pm 0.3^\circ$C for the TSP). However, the TSP measurements are in error near the leading edge of the model, as indicated by the uncertainty image.

It should be noted that TSP luminescence intensity measurements are not inherently inaccurate near model leading edges. The difficulties occur near the edge of the field of view or near sharp edges. As a result, multiple views of various portions of the model may be necessary to obtain accurate measurements over the entire model surface.

Conclusions

This paper presents an uncertainty analysis of TSP luminescence intensity measurements with CCD cameras. A general uncertainty analysis shows that the error is inversely proportional to the normalized paint sensitivity, $(-\Delta T_r/I)(\partial I/\partial \Delta T_r)$. Elemental bias and precision error sources are then described in detail, and techniques to estimate their magnitude at each pixel and to alleviate their effects are given for both standard-video and scientific-grade systems. The scientific-grade camera, although much more expensive than a standard-video camera, offers superior performance for demanding quantitative applications. Example applications of the measurement technique and uncertainty analysis to swept-cylinder and swept-wing models in supersonic flow are presented. Average uncertainty estimates of $\pm 0.3^\circ$C are obtained for several sample applications using a scientific-grade camera. However, it should be emphasized that general statements about accuracy are impossible because error estimates are quite dependent on the system parameters and test configuration. Significant variations within a single image are also quite possible. We have found that the systematic relative motion between model and illumination source is often the dominant error term. A method is proposed to alleviate the effects of model motion in transition-detection measurements. The method determines the temperature change between two run images: one at a low Reynolds number, i.e., laminar condition, and one at a higher Reynolds number. The resulting transition pattern, which would be buried in the details of an absolute temperature image, is then clearly revealed.

Acknowledgments

The first author gratefully acknowledges support received from the Flow Modeling and Control Branch of the Fluid Mechanics and Acoustics Division, NASA Langley Research Center, under Contract NAS1-20059. We would also like to thank Cecil Burkett from the Aerodynamic Measurement Branch of the Experimental Testing Technology Division at NASA Langley Research Center for performing some of the benchtop experiments, as well as Martin Morris for many insightful discussions.

References

[1]Campbell, B. T., Liu, T., and Sullivan, J. P., "Temperature Sensitive Fluorescent Paint Systems," AIAA Paper 94-2483, June 1994.

[2]Asai, K., Kanda, H., Kunimasu, T., Liu, T., and Sullivan, J. P., "Boundary-Layer Transition in a Cryogenic Wind Tunnel Using Luminescent Paint," *Journal of Aircraft*, Vol. 34, No. 1, 1997, pp. 34–42.

[3]Morris, M. J., and Donovan, J. F., "Application of Pressure- and Temperature-Sensitive Paints to High-Speed Flows," AIAA Paper 94-2231, June 1994.

[4]McLachlan, B. G., Bell, J. H., Gallery, J., Gouterman, M., and Callis, J., "Boundary Layer Transition Detection by Luminescence Imaging," AIAA Paper 93-0177, Jan. 1993.

[5]Liu, T., Campbell, B. T., Burns, S. P., and Sullivan, J. P., "Temperature- and Pressure-Sensitive Luminescent Paints in Aerodynamics," *Applied Mechanics Review*, Vol. 50, No. 4, 1997, pp. 227–246.

[6]Allison, S. W., and Gillies, G. T., "Remote Thermometry with Thermographic Phosphors—Instrumentation and Applications," *Review of Scientific Instruments*, Vol. 68, No. 7, 1997, pp. 2615–2650.

[7]Morris, M. J., Donovan, J. F., Kegelman, J. T., Schwab, S. D., Levy, R. L., and Crites, R. C., "Aerodynamic Applications of Pressure Sensitive Paint," *AIAA Journal*, Vol. 31, No. 3, 1993, pp. 419–425.

[8]Rabek, J. F., *Mechanisms of Photophysical Processes and Photochemical Reactions in Polymers: Theory and Applications*, Wiley, New York, 1987, Chap. 1.

[9]Sajben, M., "Uncertainty Estimates for Pressure Sensitive Paint Measurements," *AIAA Journal*, Vol. 31, No. 11, 1993, pp. 2105–2110.

[10]Coleman, H. W., and Steele, W. G., *Experimentation and Uncertainty Analysis For Engineers*, Wiley, New York, 1989, Chaps. 3, 4.

[11]Oglesby, D. M., Leighty, B. D., and Upchurch, B. T., "Pressure Sensitive Paint with an Internal Reference Luminophore," *Proceedings of the 41st International Instrumentation Symposium*, Instrument Society of America, Denver, CO, 1995, pp. 381–395.

[12]Liu, T., Campbell, B., and Sullivan, J., "Accuracy of Temperature-Sensitive Fluorescent Paint for Heat Transfer Measurements," AIAA Paper 95-2042, June 1995.

[13]Romano, V., Zweig, A. D., Frenz, M., and Weber, H. P., "Time-Resolved Thermal Microscopy with Fluorescent Films," *Applied Physics B*, Vol. 49, 1989, pp. 527–533.

[14]Morris, M. J., Benne, M. E., Crites, R. C., and Donovan, J. F., "Aerodynamic Measurements Based on Photoluminescence," AIAA Paper 93-0175, Jan. 1993.

[15]Bell, J. H., and McLachlan, B. G., "Image Registration for Luminescent Paint Sensors," AIAA Paper 93-0178, Jan. 1993.

[16]Donovan, J. F., Morris, M. J., Pal, A., Benne, M. E., and Crites, R. C., "Data Analysis Techniques for Pressure- and Temperature-Sensitive Paint," AIAA Paper 93-0176, Jan. 1993.

[17]"Charge-Coupled Devices for Quantitative Electronic Imaging," Photometric Ltd., Tucson, AZ, 1992.

[18]Beckwith, I. E., Creel, T. R., Jr., Chen, F.-J., and Kendall, J. M., "Freestream Noise and Transition Measurements in a Mach 3.5 Pilot Quiet Tunnel," AIAA Paper 83-0042, Jan. 1983.

G. Laufer
Associate Editor